Single-Pixel, Single-Layer Polymer Device as a Tricolor Sensor with Signals Mimicking Natural Photoreceptors

ARTICLE *in* JOURNAL OF THE AMERICAN CHEMICAL SOCIETY · SEPTEMBER 2011

Impact Factor: 12.11 · DOI: 10.1021/ja207853e · Source: PubMed

3 AUTHORS:

Vini Gautam
Australian National University
9 PUBLICATIONS **48** CITATIONS
SEE PROFILE

M. Bag
Indian Institute of Technology Roorkee
29 PUBLICATIONS **205** CITATIONS
SEE PROFILE

Ks Narayan
Jawaharlal Nehru Centre for Advanced Scien…
154 PUBLICATIONS **1,673** CITATIONS
SEE PROFILE

JACS
JOURNAL OF THE AMERICAN CHEMICAL SOCIETY

ARTICLE

pubs.acs.org/JACS

Single-Pixel, Single-Layer Polymer Device as a Tricolor Sensor with Signals Mimicking Natural Photoreceptors

Vini Gautam, Monojit Bag, and K. S. Narayan*

Chemistry and Physics of Materials Unit, Jawaharlal Nehru Centre for Advanced Scientific Research, Bangalore, India-560064.

Supporting Information

ABSTRACT: Color sensing procedures typically involve multiple active detectors or a photodetector coupled to a filter array. We demonstrate the possibility of using a single polymer layer based device structure for multicolor sensing. The device structure does not require any color filters or any subpixelation, and it distinguishes colors without any external bias. The color sensing relies on an appropriate thickness of the active polymer layer that results in a characteristic polarity and temporal profile of the photocurrent signal in response to various incident colors. The device characteristics reveal interesting similarities to the features observed in natural photosensitive systems including retinal cone cells.

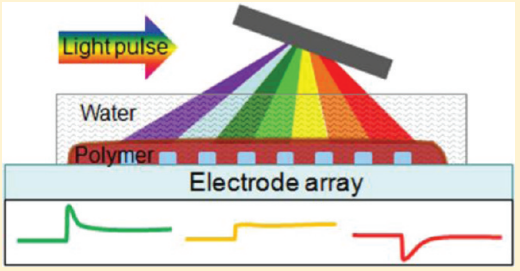

INTRODUCTION

Semiconducting polymers are an attractive choice as active materials for a variety of optoelectronic applications. The merits of these materials include facile processing routes, conformal substrates, and the choice of a wide range of absorption wavelengths (λ).[1,2] Efficient organic photodetectors consisting of binary mixtures of donor−acceptor systems, forming bulk heterojunctions (BHJs), have been demonstrated as pixel elements of large-area, color-image sensors.[3−10] The general procedure for color sensing performed in these 2-D photodiode arrays or conventional charge-coupled device (CCD) or complementary metal−oxide−semiconductor (CMOS) elements is implemented by two primary approaches. The first approach involves combining three separate elements or subpixels with photosensitivity tuned to three primary colors.[3] This approach, however, involves fabricating structures through an elaborate processing scheme. The second, more common approach involves use of a color filter array (CFA) as a mask on the monochrome sensor.[11] In this approach, the CFAs absorb a sizable percentage of the incoming light, and the color at each position must be reconstructed through interpolation algorithms (demosaicing). Relevant modifications in the red/green/blue (RGB) Bayer mosaic filters and the interpolation algorithms, along with significant improvement in pixel size and resolution, have led to striking image quality in high-end cameras.

Conceptualization of an alternative color-imaging scheme, without subpixels or CFAs and compatible with CMOS technology, has led to interesting design strategies. For example, a set of dichroic mirrors, which selectively reflect all λ values less than a cutoff, has been used in an image capture device.[12] By arranging two sets of stacked mirrors, light in different wavebands is then separated onto three identical linear CCD arrays where the light analyzed at a particular instant comes from the same source. The device design proposed by Carver Mead and co-workers at Foveon Inc. utilizes three different electrical junctions that are built at different selected depths.[13] In this case, the sizable variation of absorption coefficient in silicon with respect to λ enables the junction adjacent to the surface to collect carriers generated by blue photons; the intermediate junction collects mainly those generated by green photons, and the deeper junction collects those generated by red photons. The junctions simulate the conditions of color filters, and in the absence of physical filters, the light loss is minimized. The color reconstruction process through demosaicing is avoided, as each pixel is itself color-sensitive. Color sensing has also been demonstrated in stacked structures composed of three organic photodetectors that are individually sensitive to blue, green, and red light.[14] In this structure, the spectral response and output signal from each stacked layer are independent and correspond to the three distinct wavelengths. Taking a step further in this line of thought, we propose and demonstrate a polymer BHJ-based, single-pixel, single-layer structure (instead of multiple-layer stacks) that is capable of distinguishing multiple colors without an external bias. The methodology essentially relies on the introduction of an aqueous layer in the device, which results in wavelength-specific transient characteristics and polarity of the response upon photoexcitation. We do not propose a new imaging scheme but introduce a type of photodetector whose color response characteristics resemble features observed in visual processes.

BHJ structures, consisting of an interpenetrating network of electron donor- and acceptor-type polymers, have been widely adopted in contemporary research associated with organic solar cells, where charge transfer takes place between a photoexcited donor and an acceptor within an ultrafast time scale, followed by charge separation and transport processes at longer time scales. In the present studies, we use a regioregular alkylthiophene as the

Received: August 19, 2011

dx.doi.org/10.1021/ja207853e | J. Am. Chem. Soc. XXXX, XXX, 000–000

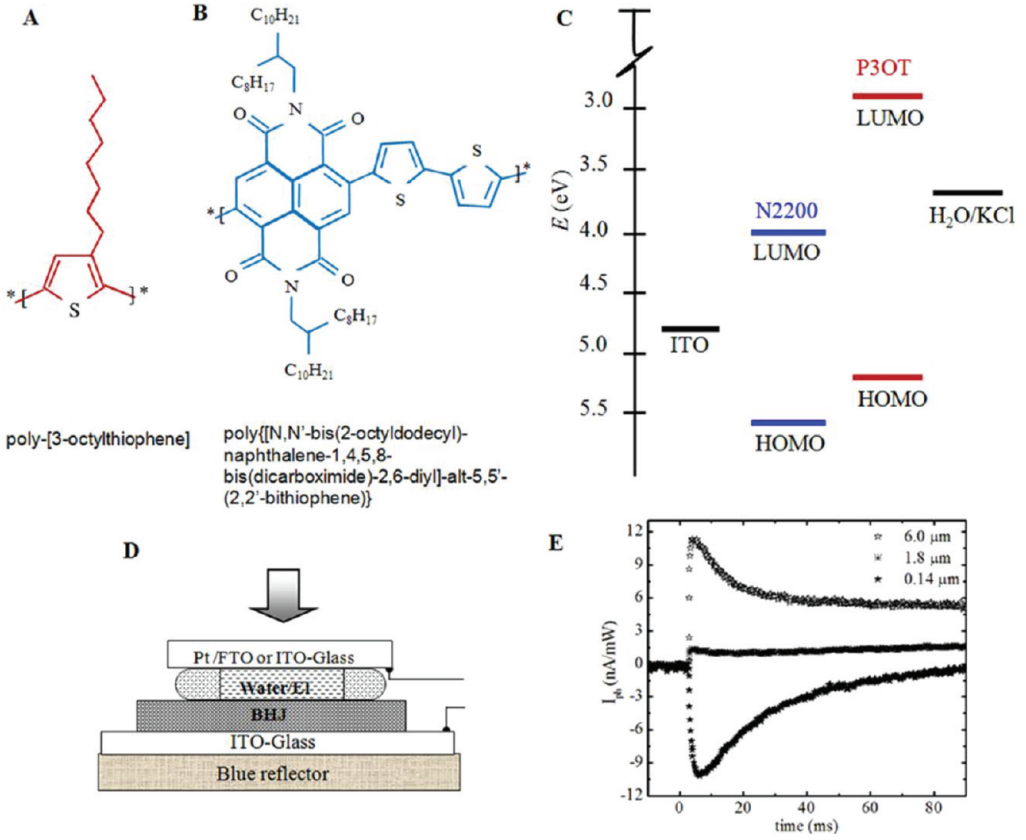

Figure 1. Structures of (A) poly(3-octylthiophene) (P3OT) and (B) N2200 polymers used to form the BHJ layer. (C) Absolute energy levels of indium tin oxide (ITO), P3OT, and N2200 and redox potential of water and aqueous KCl. HOMO = highest occupied molecular orbital; LUMO = lowest occupied molecular orbital. (D) Experimental setup and device structure for ITO|BHJ|aq device. The blue reflector is used for the three-color detector configuration. (E) Dependence of photocurrent (I_{ph}) on thickness of the BHJ layer for λ = 525 nm (green). The light flash is switched on at t = 0 s.

donor and the stable N2200[15] as the acceptor (instead of $PC_{60}BM$) for the BHJ forming layer. The chemical structure and energy levels of the materials used are shown in Figure 1A−C. The stability of such polymer films in contact with water and aqueous electrolytes has been indicated by results based on ultrafast photoexcitation spectroscopy techniques.[16] Poly(3-hexylthiophene) (P3HT) has also been shown to be stable in contact with deionized water in a water-gate field effect transistor geometry.[17] The use of water and aqueous electrolytes (which do not constitute a regenerative redox couple) serves as an effective barrier interface in the device, which modifies the electronic photocurrent to characteristic transient profiles, besides mimicking the environment offered by physiological buffer solutions involved in natural vision systems. Even though the phototransduction efficiencies of these devices are low, we highlight the biological resemblance of the signals emanating from such device structures and demonstrate a simple color-sensing vision system. Such visual photoreceptor-type sensors operating in an aqueous environment can be used as stimulation elements upon interfacing with other retinal neurons like the ganglion cells.

Recent studies on the thickness dependence of the photovoltage (V_{ph}) from BHJ|aq(KCl) structures[18] revealed features that are utilized in the present context to create a λ-dependent signal. The $V_{ph}(t)$ and photocurrent (I_{ph}) profile is controlled by a combination of factors including the BHJ|aq interfacial boundary condition, asymmetry in the electron and hole transport, and vertical distribution gradients of donor and acceptor components. In effect, for thick BHJ films (>2 μm), the $I_{ph}(t)$ generated across the BHJ|aq upon photoexcitation (for all λ) consists of a positive response, while devices with BHJ film having thickness less than a critical thickness give rise to a negative transient signal. Here we demonstrate distinct characteristics of $I_{ph}(t)$ upon photoexcitation at λ values corresponding to the three primary colors, red, green and blue, upon use of an appropriate (or critical) thickness of the BHJ film in the same BHJ|aq device structure, as shown in Figure 1D.

RESULTS

Arriving at the Conditions Required for Two-Color Sensing. Convergence to the optimum thickness of the BHJ layer can be systematically reached by monitoring the signal from the device at a specific λ. Upon measuring the photoresponse in short-circuit and open-circuit conditions, it was observed that the photocurrent mode exhibits a transient signal while the photovoltage mode displays a steady-state potential with the same polarity as that of the current (see Figure S1in Supporting Information). Figure 1E indicates the trend of $I_{ph}(t)$ as a function of thickness at λ = 525 nm. It is observed that photoillumination of a thick BHJ film ($\approx$ 6 μm) results in a positive $I_{ph}(t)$ spike, while photoillumination of a thin film ($\approx$ 0.14 um) results in a negative spike. These measurements were extended for λ = 690 nm. Upon examining the results, it was noted that there existed a range of thickness ($\approx$2 μm for 4:1 donor:acceptor ratio) where λ = 525 nm

dx.doi.org/10.1021/ja207853e |J. Am. Chem. Soc. XXXX, XXX, 000–000

and λ = 690 nm incident lights gave rise to signals with contrasting polarity (positive and negative, respectively). This criterion of appropriate thickness forms the basis for fabricating a two-color detector, where identification of blue/green and red colors is based on opposite polarity of $I_{ph}(t)$ of substantial magnitude ($\sim$ 5 nA/mW) (Figure 2). The phenomenon of two-color sensing was operational for a wide range of intensities (2 μW/cm^2 to 20 mW/cm^2), operable in white background light (see Figure S2 in Supporting Information), and reproducible over extended cycles of operation (see Figure S3 in Supporting Information). It should be noted that the device response is similar when deionized water is used in place of an electrolyte (see Figure S4 in Supporting Information). The absence of salt increases the stability of the polymer medium by minimizing photoelectrochemical processes at the interface.

Three-Color and Multicolor Sensing Using Characteristic Response Features. The binary logic procedure naturally is restrictive and is not sufficient for three-level primary color sensing. However, it is noticed from the $I_{ph}(t)$ measurements that the dynamics of the current rise and decay for the two colors, blue/green and red, are quite different. This difference in the dynamics, along with a choice of a substrate, which can bring in selectivity in the form of an additional reflection of a color band, can be utilized to elicit a distinct response to create three-level logic. Using the appropriate thickness of the BHJ layer and a blue-selective reflector as the substrate, a three-color detection scheme based on single-pixel, single-layer, and filter-free optics appears possible, as shown in Figure 3A. It should be noted that variation of the peak value of $I_{ph}(t)$ as a function of intensity of incident light is observed to be linear at low intensities, while it saturates at higher values and follows sublinear behavior (Figure 3A, inset).

The three-color detection scheme can be formulated upon numerically representing the response pulse. For example, the response to λ = 525 nm can be expressed as$(1 - e^{-t/\tau_1})\, e^{-t/\tau_2}$. The time constants τ_1 and τ_2 characterize the rise and decay dynamics of positive $I_{ph}(t)$. The response to λ = 690 nm can be similarly expressed as $-(1 - e^{-t/\tau_3})e^{-t/\tau_4}$. The time constants τ_3 and τ_4 characterize the rise and decay dynamics of the negative $I_{ph}(t)$. In the case of incident blue light in the presence of a Bragg reflector (λ = 470 nm) on the substrate, the response can be expressed in the form of an algebraic summation of the terms for λ = 525 nm and λ = 690 nm along with an additional prefactor a and an offset term b: that is, $I_{ph}(t) = (1 - e^{-t/\tau_1})e^{-t/\tau_2} - a\,(1 - e^{-t/\tau_3})e^{-t/\tau_4} + b$. The relative magnitudes of the fitting parameters as a function of λ are given in Table S1 (see Supporting Information). Such analog model formalism can possibly be used as a demosaicing tool for three-color detection. The uniqueness of the analog representation further implies that a natural pure color can be distinguished from an additive color; that is, the response to an incident pure-yellow light is different from a response to yellow color obtained from a combination of red and green (CIE 1931 color space chromaticity diagram). Such a comparison from the BHJ|aq device response is depicted in Figure 3B. Furthermore, the $I_{ph}(t)$ response to illumination with white light does not exhibit the transient spikes observed with monochromatic pulses (see Figure S5 in Supporting Information).

The pulse profile analysis to arrive at a color definition is not a constrained procedure and exhibits features such as an inherent larger tolerance for a color detection scheme over a large intensity (I) variation range. The curve-fitting parameters have characteristic

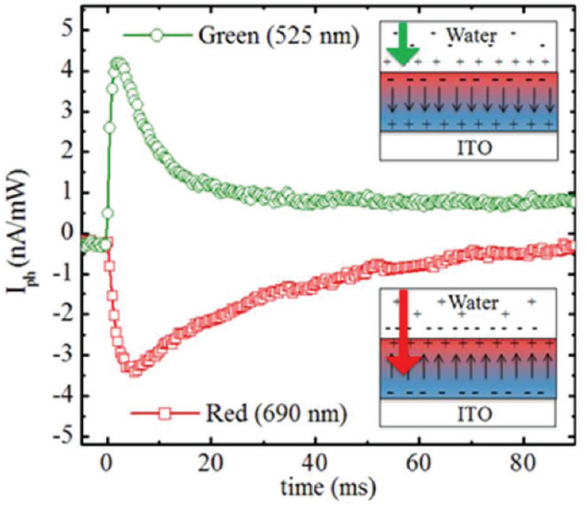

Figure 2. Normalized photoresponse of ITO|P3OT:N2200|aq device in a two-color (red and green) detector configuration. The thickness of the BHJ film is $\approx$2 μm, and the light flash is switched on at t = 0 s. The schematics in the insets depict the mechanism of polarity reversal in response to green (high-absorbing) and red (low-absorbing) λ values. The color gradient depicting the BHJ layer between water and ITO represents the vertical phase segregation of donor and acceptor with acceptor concentration gradient toward the ITO.

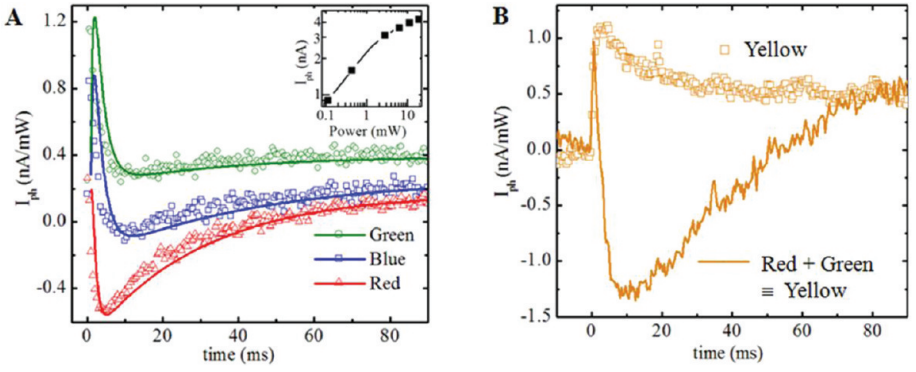

Figure 3. (A) Photoresponse of a three-color (red, blue, green) detector device fabricated with a blue-selective (λ = 470 nm) Bragg reflector behind the ITO-coated glass. The solid lines correspond to the analog fit to the observed I_{ph} (see text). (Inset) Variation of the peak value of $I_{ph}(t)$ as a function of incident intensity λ = 532 nm. (B) Response of ITO|BHJ|aq(KCl) device structure to spectral yellow light (575 nm) and to the yellow color obtained from optically mixing the red (690 nm) and green (525 nm) colors. Thickness of the BHJ layer is $\approx$2.1 μm. The light flash is switched on at t = 0 s.

dx.doi.org/10.1021/ja207853e |J. Am. Chem. Soc. XXXX, XXX, 000–000

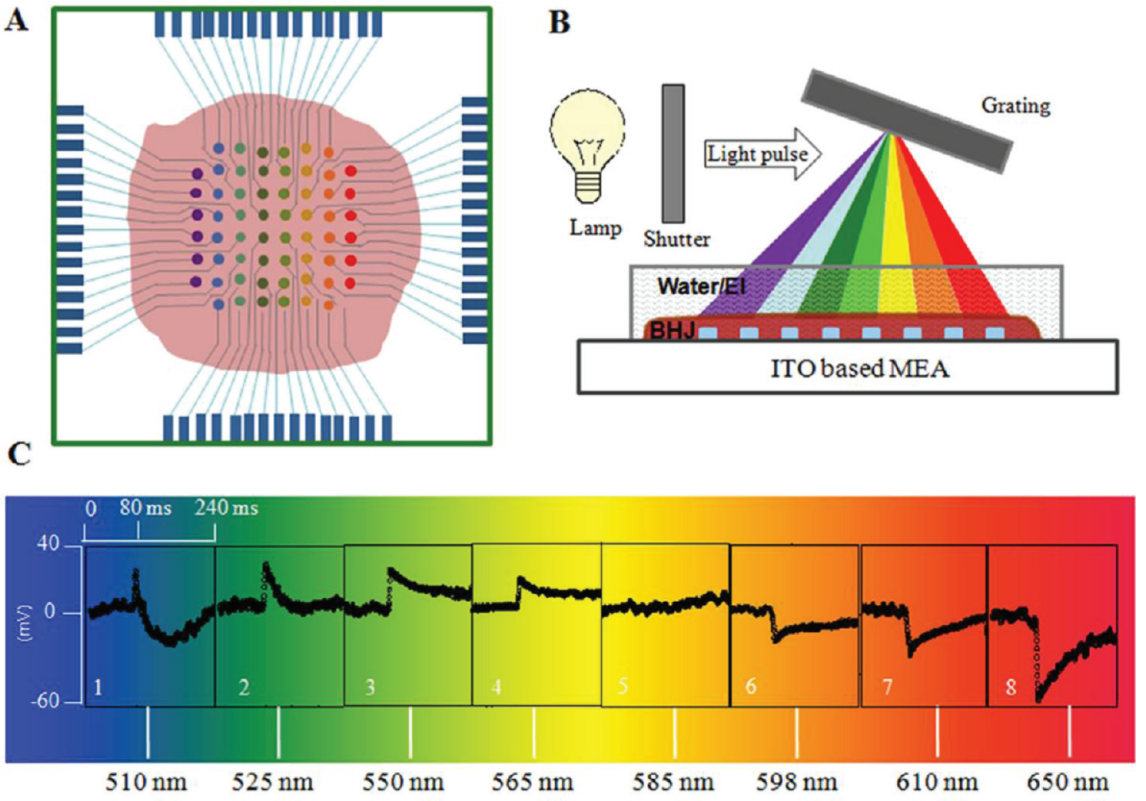

Figure 4. (A) Schematic of the 8 × 8 multielectrode array (MEA) with 60 ITO electrodes coated with the BHJ layer of thickness ≈2 μm (equal to L_c, see text). Aqueous KCl solution (100 mM) is held on top of the polymer film. (B) Various wavelengths of the visible spectrum dispersed onto the array in the manner shown. (C) Photovoltage response of the ITO|P3OT:N2200|aq device as a function of various λ values of the visible spectrum (λ error bar ~10 nm). The light flash is switched on at 80 ms. Eight windows correspond to the responses from each row of the MEA.

dependence on I, where τ_2 and τ_4 scale inversely ($\propto -\log I$) and a varies in a power-law manner ($\propto I^p$, where $p \sim 0.2-0.5$). The large dynamic range observed in the λ-dependent response of BHJ|aq systems enables digital signal processing and offers a simple, practical procedure to define the color. A digital logic circuit with comparators can further provide signal processing and demosaicing to arrive at the color information (see Figure S6 in Supporting Information).

The variation in pulse response parameters as a function of λ in the entire visible range can be gauged by dispersing white light and having it incident on a patterned substrate (Figure 4A,B). The patterned structure consists of a multielectrode array (MEA) consisting of 60 ITO electrodes forming a square (8 × 8) layout, each of which are connected to an amplifier. Upon casting the BHJ film of appropriate thickness onto the MEA and using 100 mM aqueous KCl, the amplified response from each electrode recorded is shown in Figure 4C. Notice that each pixel response in a given row of the MEA has unique characteristics. The typical wavelength resolution estimated for the measurement parameters is limited by the differential sensitivity of the device, which is maximum around the wavelength range 600−630 nm, around which the polarity change is observed (see Figure S7 in Supporting Information). The array results indicate the uniqueness in the response to specific colors. The results validate the utility of a single pixel to decipher a color over a wide range since positive and negative polarity signals are not identical and do not compensate to arrive at a zero magnitude. On the basis of response profiles from the array and reflection attributes of the substrate, the color discrimination resolution of the single-pixel color sensor over the range 400 nm < λ < 700 nm can be on the order of ~10 nm.

DISCUSSION

The origin of the polar nature of signals from the BHJ|aq-based devices can be understood by differences in the rate of carrier accumulation at the BHJ|aq interface and ITO|BHJ interface. The large prominent spikes associated with the initial response to the photoexcitation arise from the barrier that facilitates charge accumulation at the BHJ|aq interface and the dynamics associated with hole collection at the ITO electrode. The thickness of the BHJ layer and the absorption coefficient of the incident light, $\alpha(\lambda)$, then are crucial tuning parameters for color discrimination. Photoexcitation of thick polymer films from the aqueous-layer side (for all λ) results in generation of charge carriers largely at the BHJ|aq interface and hole diffusion toward the BHJ|ITO interface, resulting in positive polarity of $I_{ph}(t)$. For thin polymer layer devices (<~ 200 nm), the higher rate of accumulation of excess negative charge carriers at the BHJ|ITO interface results in negative polarity of $I_{ph}(t)$ over the relevant temporal range of measurement (>1 ms). We exploit this thickness-dependent polarity reversal by arriving at the optimum film thickness where photoexcitation by a high- and low-absorbing λ appears in the form of polarity reversal. Consequently, at the critical thickness (~2 μm), the charge carrier generation due to shorter λ (blue/green) produces a positive polarity of $I_{ph}(t)$, while higher λ (red) produces a negative polarity of $I_{ph}(t)$. It should be noted that the value of the critical thickness is

dx.doi.org/10.1021/ja207853e |J. Am. Chem. Soc. XXXX, XXX, 000–000

inversely dependent upon the concentration of N2200 in the BHJ layer and can be utilized for tuning the device; for instance, the critical thickness for the BHJ with 4:1 P3OT:N2200 composition is ~2 μm while the value for a 1:1 ratio was observed to be ~200 nm.

The positive steady-state photocurrent upon illumination with shorter λ (blue/green) can arise from the energetically possible photoinduced electron transfer from the BHJ layer to the aqueous layer (Figure 1C). The explanation of the BHJ layer as a photoelectrode has been utilized previously in the context of interfacial redox processes.[19] The small magnitude of the steady-state current, prolonged stability, and lower intensity in the present case, however, points to a relatively smaller contribution from these processes.

The thickness and λ-dependent polarity reversal of $I_{ph}(t)$ appears to be present only in certain combination of donor−acceptor systems; for instance, the features were not noticed in carbazole-based PCDTBT donor systems.[18] The absence of these features in P3HT devices with [6,6]-phenyl-C61-butyric acid methyl ester (PCBM) as acceptors suggests the importance of vertical phase separation in P3HT:N2200 blends and the enrichment of acceptor distribution away from the aqueous layer interface. The vertical distribution and interface layer composition is evident upon comparing the response of BHJ|aq devices with those of P3OT|N200|aq and N2200|P3OT|aq bilayer structures (see Figure S8 in Supporting Information). This type of vertical distribution further appears to be consistent with the low power conversion efficiency and low quantum yield (<15%) obtained for P3HT:N2200 solar cells.[20] Note that, unlike PCBM, N2200 is a polymer with a tendency to form an organized microstructure.[21,22] In the case of light with λ in the low-absorption region (690 nm) incident from the aqueous side of the BHJ(P3HT:N2200)|aq structure, absorption in the vicinity of ITO|BHJ with a predominant acceptor network then can result in electron accumulation at this interface, resulting in a negative $I_{ph}(t)$ transient. The dominant diffusion process rather than drift process in the thick active layer, along with the distribution gradient of the two polymer phases, is the key to arrive at color-selective signals. This physical process, including the central feature of polarity reversal for green and red light illumination (schematically represented in Figure 2, inset), is consistent with all the observations. Furthermore, upon illumination with white light, the generation of charge carriers is comparatively more uniform in the bulk of the BHJ layer, resulting in the absence of transient features in $I_{ph}(t)$ (Figure S5, Supporting Information). In order to discriminate between the blue and green color responses, we note the fact that illumination from the ITO|BHJ side results in a negative polarity of $I_{ph}(t)$ and $V_{ph}(t)$.[18] The presence of the λ-selective reflector (470 nm) on the rear side of the ITO-coated substrate (Figure 1D) results in a characteristic signal, that is, a positive $I_{ph}(t)$ followed by a negative $I_{ph}(t)$ for $\lambda \sim 470$ nm.

Note that, in the absence of the aqueous layer and hence the interfacial barrier in a solid-state device, the negative polarity as well as the sharp transient spikes are absent and a huge steady-state photocurrent is observed (Figure 5). Furthermore, $I_{ph}(t)$ arising from diffusion processes in ITO|BHJ|aq devices is lesser in magnitude compared to solid-state devices due to the presence of the BHJ|aq interface, which causes accumulation of charge carriers and promotes recombination under constant illumination. The contribution of such bimolecular recombination processes can be observed by noting the asymmetry in the charging and discharging photocurrent signal profile.

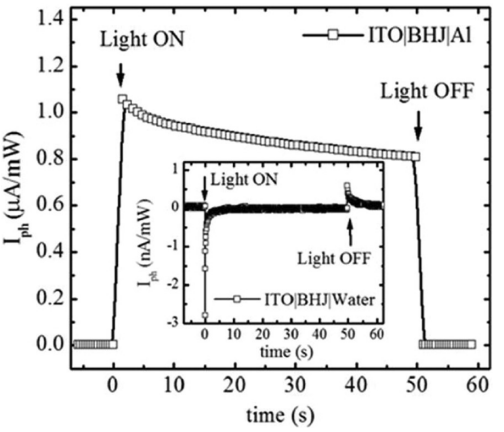

Figure 5. Comparison of BHJ|aq device response with that of a solid-state device. (Inset) Response of ITO|BHJ|aq(water) and ITO|BHJ|aluminum device with λ = 525 nm from the ITO side, where the thickness of the BHJ layer is ~450 nm.

The dynamics involved in the device response can be modeled to arise from the combination of intrinsic processes and the macroscopic equivalent circuit parameters.[18,23] The net current arising due to the electronic and hole transport in the polymer bulk in response to photoexcitation can be simulated by use of a current source whose polarity is dependent on λ and other relevant circuit parameters (see Figure S9 in Supporting Information). Furthermore, the parameters of quantum efficiency and the spectral sensitivity curves used to characterize conventional photodetectors and colorimeters are not directly applicable for comparison with the present devices, since the figures of merit deciding the pulse parameters in BHJ|aq devices are quite different. The spectral range of operation, however, covers the entire visible range as seen in the modulated photocurrent action spectrum of ITO|BHJ|aq detectors (see Figure S10A in Supporting Information). Furthermore, the observed time scales in the millisecond range are suitable for designing simple analog electronic circuits.

We further highlight the similarities of BHJ|aq based photodetectors to certain biological systems. Polarity-dependent color discrimination procedure has been previously demonstrated in systems completely different from BHJ|aq: (i) In the purple membrane proteins, bacteriorhodopsin (bR) and its analogues, there exists a photochemical cycle in response to light, which results in displacement currents. The λ-dependent direction of the displacement currents then determines the polarity of $I_{ph}(t)$ and $V_{ph}(t)$ across the oriented membranes.[24,25] (ii) In photosynthetic membranes with chlorophyll, the polarity of $I_{ph}(t)$ in strong light-absorbing regions and weak light-absorbing regions is observed to be opposite.[26] This polarity difference arises from the complex refractive indices of the various layers involved in the suspended membranes.[27] In the present case, the responsivity of the BHJ|aq structures is at least an order of magnitude higher compared to these systems, along with a higher degree of control for the device parameters and more facile fabrication procedure.

It is also interesting to note that the time scales and magnitudes of the signals obtained from BHJ|aq structures are similar to those obtained from the electrochemical recording of bR monolayers as well as electrophysiological recording of an isolated mammalian retina (Figure 6). Detection frequencies (10−20 Hz) and detection thresholds (~ 5 μW/cm^2) of BHJ|

dx.doi.org/10.1021/ja207853e |J. Am. Chem. Soc. XXXX, XXX, 000–000

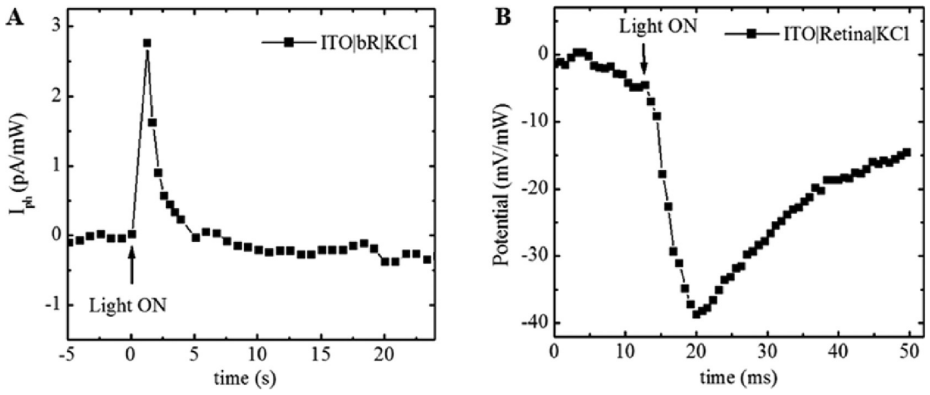

Figure 6. (A) Transient photocurrent across an ITO|bR|aq(100 mM KCl) device. (B) ERG recording from an isolated retina by use of a multielectrode array.

aq devices are also comparable to those in primate vision systems at the receptor and perception levels, respectively.[28] The variation of $V_{ph}(t)$ and $I_{ph}(t)$ arising from the BHJ|aq devices as a function of intensity of the incident light is also similar to the dependence observed in visual processes of certain nonvertebrate and vertebrate photoreceptors.[29,30]

Advances have been made in the use of microphotodiode arrays[31] and patterned stimulation electrodes[32,33] for artificial retina devices designed to address various vision-related diseases such as retinal pigmentosa or to augment normal vision. However, known artificial retina devices involve conventional electronics that are based on inorganic materials such as carbon nanotubes or silicon or platinum/iridium oxide coated substrates.[31−35] The choice of biocompatible photoactive optoelectronic polymers may have an intrinsic advantage toward this application. The stimulation threshold levels involved within these neuronal layers are on the order of a few millivolts, similar in magnitude to those arising from the BHJ|aq structures. The potentials arising from the conjugated polymer/electrolyte interface have been recently utilized for stimulation of hippocampal neurons cultured onto the polymer surfaces.[36] Charge displacement within the polymeric bulk upon photoexcitation induces ion redistribution at the electrolytic/neuronal membrane interface, thus leading to membrane depolarization with subsequent action potential generation in these neurons. Furthermore, a combination of three semiconducting polymers tuned to different spectral ranges can perform in vitro the task of natural photoreceptors in the framework of the trichromatic theory of color vision, that is, color detection by considering three types of cone photoreceptors, S, M, and L, with peak spectral sensitivities at around 430, 530, and 560 nm, respectively.[37]

The fuzzy logic nature of the single-pixel response for color interpretation from our $I_{ph}(t)$ measurements can possibly be mapped to a combination of low-end photoreceptor process and higher-end neural processes. In natural vision process, the signals arising from the S, M, and L cones undergo complex processing at the ganglion cell level, and this is understood on the basis of opponent-process theory of color recognition. This model explains the color vision at the perception level with its main postulate being that the visual system interprets color in an antagonistic way: red versus green, blue versus yellow, and black versus white.[37,38] Analysis of the photosignals from the BHJ|aq structures appears to resemble certain outcomes from this antagonistic theory. For instance, the opposite-polarity response from the red and green/blue can be equated to the antagonistic effect of the L/M cones. Furthermore, photosignals from BHJ|aq devices reveal higher sensitivity to blue color in a red background and higher sensitivity to red color in a blue background (see Figure S10B in Supporting Information). Such an effect of the background light persists for a finite duration corresponding to the space charge relaxation. The outcome of this effect is similar to chromatic adaptation in the visual system, where prior exposure to red light results in higher sensitivity to green color and vice versa.[39]

The modest frame rates and the wide color discrimination range of BHJ|aq devices may be adequate for certain sensor applications. While the pulse-profiling scheme may be unique for a color discrimination procedure with attributes such as identification of the spectral purity of a given source, it may have a limitation in resolving a color in situations with simultaneous colors and large intensity variation. It may, however, be possible to overcome this limitation with additional device-optimization and refined data/image processing algorithms.

CONCLUSION

We have demonstrated a novel color discriminator device consisting of a single active BHJ layer of appropriate thickness in contact with an aqueous medium. The device response to an incident color is associated with a polarity and a unique set of parameters describing the transient output. The stability of the BHJ polymers in contact with aqueous media, as well as the interesting similarities of photoresponse of such structures with that of the natural vision systems, demonstrates that organic electronics and optoelectronics offer some credible alternatives to materials utilized in artificial retina solutions. Further studies on issues such as biocompatibility and the prospect of seamless integration of these devices with neural systems hold a promising route for a variety of optoelectronic applications.

EXPERIMENTAL SECTION

Materials and Device Fabrication. Poly(3-octylthiophene) (P3OT) obtained from Sigma Aldrich was used as the donor-type polymer, while poly{[*N*,*N*′-bis(2-octyldodecyl)naphthalene-1,4,5,8-bis-(dicarboximide)-2,6-diyl]-*alt*-5,5′-(2,2′-bithiophene)} (N2200) obtained from PolyeraActivInk was used as the acceptor-type polymer. Both polymers were used without additional purification. The blends of P3OT and N2200 were prepared in different ratios (w/w) with chlorobenzene as

dx.doi.org/10.1021/ja207853e |*J. Am. Chem. Soc.* XXXX, XXX, 000–000

the solvent (10 mg/mL concentration). The results presented are for BHJ of composition 4:1 P3OT:N2200. The BHJ solution was drop-cast on precleaned indium−tin oxide (ITO) coated glass substrates (∼20 Ω/□) for thick films (∼400 nm−6 μm), while thinner films (∼200 nm) were made by spin-casting the blend solution on the substrate at 1000 rpm speed for 100 s. In order to achieve critical thickness (2 ± 0.3 μm), 10 μL volume of the BHJ solution was drop-cast from a fixed height of 20 mm onto the ITO substrates, preheated at 100 °C for 5 min. All devices were fabricated inside a glovebox (Mbraun Inc.)ernd cured at 110 °C for 10 min. Deionized water and aqueous KCl (100 mM concentration) was used as electrolytes. Poly(dimethylsiloxane) (PDMS) wells (diameter ≈1.5 mm) were used to confine the aqueous medium on the polymer film. Platinum-coated fluorine-doped tin oxide (FTO) or ITO glass was used as counterelectrode in contact with aqueous layer and was maintained at ground potential for all measurements. The thickness of the films was measured on a Dektak stylus profilometer (Veeco Instruments) with 3 mg force, 12.5 μm tip size, and measurement error of ∼50 nm.

Photocurrent Recording. Light-emitting diodes (LEDs) driven by a frequency generator (Sony Tektronix AFG320) were used as light sources. The LED spectra were measured using a spectrometer (Hamamatsu TM-VIS/NIR-CCD C10083CA). Devices were photoilluminated from the BHJ|aq side. The $I_{ph}(t)$ response across the ITO|BHJ|aq structures was recorded with a LeCroy (Waverunner6100A) oscilloscope across a 1 MΩ coupling resistor in the dc mode or with an electrometer (Keithley 6512) for low current magnitudes. Intensity dependence studies were carried out with a set of neutral density filters with a 532 nm laser.

Multicolor Sensing with Multielectrode Arrays. Recordings were done with MEAs with 60 ITO electrodes of 40 μm diameter and 200 μm interelectrode spacing in an 8 × 8 arrangement (obtained from Ayanda Biosystems). The electrode area of the MEA was coated with the polymer BHJ blend. The MEA was then annealed at 70 °C for 20 min and mounted onto the MEA1060-BC current−voltage amplifier (MultichannelSystems). KCl solution (100 mM) was used as the electrolyte, and Ag/AgCl pellet was used as the counter (ground) electrode. White light source focused onto a monochromator grating was used to obtain the visible spectrum onto the MEA. The data were acquired at a sampling rate of 25 kHz by use of a 16-channel data acquisition card and MC_Rack software (Multichannel Systems).

Electrical Recordings from Bacteriorhodopsin Monolayers and Isolated Retina. Bacteriorhodopsin (bR) monolayers were prepared via layer-by-layer assembly of wild-type bR (obtained from MIB Inc.) on precleaned ITO substrates. The transient photoelectric response of unoriented bR monolayer devices in the ITO|bR|KCl geometry was measured with an electrometer and a monochromatic laser light pulse of 532 nm. Retinal whole mounts were prepared by standard protocols with mice (BL6J/C57). The explanted retina was placed ganglion side down onto the MEA with 60 ITO electrodes of 40 μm diameter and 200 μm interelectrode spacing in an 8 × 8 arrangement (obtained from Ayanda Biosystems), mounted into MEA1060-BC voltage amplifier (Multichannel Systems). Ames' medium (Sigma Aldrich) was used as the nutrient and buffer medium for the retina, and Ag/AgCl pellet was used as the counter (ground) electrode. White LED, driven by a function generator (Sony Tektronix AFG320), was used for photostimulation of the retina from the electrolyte side of the MEA. The V_{ph} data was acquired by use of a 16-channel data acquisition card and MC_Rack software (Multichannel Systems) at a sampling frequency of 25 kHz. The ERG shown depicts only the a-wave arising from stimulation of the photoreceptor layer in the retina.

■ ASSOCIATED CONTENT

Ⓢ Supporting Information. Ten figures, showing comparison between photovoltage and photocurrent mode of operation, color detection in white background, stability of BHJ|aq-based photodetectors, comparison of water and KCl as aqueous media for response to white color, photoresponse of ITO|BHJ|aq-(water) device to white, red, and green light, proposed electronic circuit for demosaicing, differential sensitivity as a function of wavelength, photoresponse of bilayer structures, simulation of two-color detection scheme by use of circuit parameters, and modulated photocurrent spectrum of BHJ|aq photodetectors, and one table of parameter values for the mathematical fit for three-color detection. This material is available free of charge via the Internet at http://pubs.acs.org.

■ AUTHOR INFORMATION

Corresponding Author
narayan@jncasr.ac.in

■ REFERENCES

(1) Forrest, S. R. *Nature* **2004**, *428*, 911–918.
(2) Clark, J.; Lanzani, G. *Nat. Photonics.* **2010**, *4*, 438–446.
(3) Antognazza, M. R.; Scherf, U.; Monti, P.; Lanzani, G. *Appl. Phys. Lett.* **2007**, *90*, No. 163509.
(4) Chen, E.; Chang, C. Y.; Shieh, J. T.; Tseng, S. R.; Meng, H. F.; Hsu, C. S.; Horng, S. F. *Appl. Phys. Lett.* **2010**, *96*, No. 043507.
(5) Gong, X.; Tong, M. H.; Xia, Y. J.; Cai, W. Z.; Moon, J. S.; Cao, Y.; Yu, G.; Shieh, C. L.; Nilsson, B.; Heeger, A. J. *Science* **2009**, *325*, 1665–1667.
(6) Halls, J. J. M.; Walsh, C. A.; Greenham, N. C.; Marseglia, E. A.; Friend, R. H.; Moratti, S. C.; Holmes, A. B. *Nature* **1995**, *376*, 498–500.
(7) Punke, M.; Valouch, S.; Kettlitz, S. W.; Christ, N.; Gartner, C.; Gerken, M.; Lemmer, U. *Appl. Phys. Lett.* **2007**, *91*, No. 071118.
(8) Schilinsky, P.; Waldauf, C.; Brabec, C. J. *Appl. Phys. Lett.* **2002**, *81*, 3885–3887.
(9) Wang, X.; Hofmann, O.; Das, R.; Barrett, E. M.; deMello, A. J.; deMello, J. C.; Bradley, D. D. C. *Lab Chip* **2007**, *7*, 58–63.
(10) Nalwa, K. S.; Cai, Y.; Thoeming, A. L.; Shinar, J.; Shinar, R.; Chaudhary, S. *Adv. Mater.* **2010**, *22*, 4157–4161.
(11) Yu, G.; Srdanov, G.; Wang, J.; Wang, H.; Cao, Y.; Heeger, A. J. *Synth. Met.* **2000**, *111*, 133–137.
(12) Vincent, K. D. (Cupertino, CA); Neumann, H. D. (Los Altos, CA). Color combiner and separator and implementations. U.S. Patent 4,870,268, 1989.
(13) Merrill, R. B. (Woodside, CA). Color separation in an active pixel cell imaging array using a triple-well structure. U.S. Patent 5,965,875, 1999.
(14) Seo, H.; Aihara, S.; Watabe, T.; Ohtake, H.; Kubota, M.; Egami, N. *Jpn. J. Appl. Phys. 2* **2007**, *46*, L1240–L1242.
(15) Chen, Z.; Zheng, Y.; Yan, H.; Facchetti, A. *J. Am. Chem. Soc.* **2009**, *131*, 8–9.
(16) Antognazza, M. R.; Ghezzi, D.; Musitelli, D.; Garbugli, M.; Lanzani, G. *Appl. Phys. Lett.* **2009**, *94*, No. 243501.
(17) Kergoat, L.; Herlogsson, L.; Braga, D.; Piro, B.; Pham, M.-C.; Crispin, X.; Berggren, M.; Horowitz, G. *Adv. Mater.* **2010**, *22*, 2565–2569.
(18) Gautam, V.; Bag, M.; Narayan, K. S. *J. Phys. Chem. Lett.* **2010**, *1*, 3277–3282.
(19) Abe, T.; Nagai, K. *Org. Electron.* **2007**, *8*, 262–271.
(20) Fabiano, S.; Chen, Z.; Vahedi, S.; Facchetti, A.; Pignataro, B.; Loi, M. A. *J. Mater. Chem.* **2011**, *21*, 5891–5896.
(21) Schuettfort, T.; Huettner, S.; Lilliu, S.; Macdonald, J. E.; Thomsen, L.; McNeill, C. R. *Macromolecules* **2011**, *44*, 1530–1539.
(22) Rivnay, J.; Toney, M. F.; Zheng, Y.; Kauvar, I. V.; Chen, Z.; Wagner, V.; Facchetti, A.; Salleo, A. *Adv. Mater.* **2010**, *22*, 4359–4363.
(23) Bag, M.; Narayan, K. S. *Phys. Rev. B* **2010**, *82*, 075308.
(24) Boyer, A.; Dery, M.; Selles, P.; Arbour, C.; Boucher, F. *Biosens. Bioelectron.* **1995**, *10*, 415–422.

(25) Lörinczi, É.; Verhoefen, M.-K.; Wachtveitl, J.; Woerner, A. C.; Glaubitz, C.; Engelhard, M.; Bamberg, E.; Friedrich, T. *J. Mol. Biol.* **2009**, *393*, 320–341.
(26) Gräber, P.; Trissl, H. W. *FEBS Lett.* **1981**, *123*, 95–99.
(27) Paillotin, G.; Dobek, A.; Breton, J.; Leibl, W.; Trissl, H. W. *Biophys. J.* **1993**, *65*, 379–385.
(28) Loop, M. S.; Crossman, D. *Visual Neurosci.* **2000**, *17*, 119–125.
(29) Lisman, J. E.; Brown, J. E. *J. Gen. Physiol.* **1975**, *66*, 473–488.
(30) Bader, C. R.; MacLeish, P. R.; Schwartz, E. A. *Proc. Natl. Acad. Sci. U.S.A.* **1978**, *75*, 3507–3511.
(31) Chow, A. Y.; Chow, V. Y.; Packo, K. H.; Pollack, J. S.; Peyman, G. A.; Schuchard, R. *Arch. Ophthalmol.* **2004**, *122*, 460–469.
(32) Humayun, M. S.; Weiland, J. D.; Fujii, G. Y.; Greenberg, R.; Williamson, R.; Little, J.; Mech, B.; Cimmarusti, V.; Van Boemel, G.; Dagnelie, G.; de Juan, E. *Vision Res.* **2003**, *43*, 2573–2581.
(33) Rizzo, J. F.; Wyatt, J.; Loewenstein, J.; Kelly, S.; Shire, D. *Invest. Ophthal. Visual Sci.* **2003**, *44*, 5355–5361.
(34) Butterwick, A.; Huie, P.; Jones, B. W.; Marc, R. E.; Marmor, M.; Palanker, D. *Exp. Eye Res.* **2009**, *88*, 22–29.
(35) Shoval, A.; Adams, C.; David-Pur, M.; Shein, M.; Hanein, Y.; Sernagor, E. *Front. Neuroeng.* **2010**, *3*, 12.
(36) Ghezzi, D.; Antognazza, M. R.; Dal Maschio, M.; Lanzarini, E.; Benfenati, F.; Lanzani, G. *Nat. Commun.* **2011**, *2*, 166.
(37) Solomon, S. G.; Lennie, P. *Nat. Rev. Neurosci.* **2007**, *8*, 276–286.
(38) Nassi, J. J.; Callaway, E. M. *Nat. Rev. Neurosci.* **2009**, *10*, 360–372.
(39) Boynton, R. M. *J. Opt. Soc. Am.* **1956**, *46*, 172–179.